Electron paramagnetic resonance studies of cobalt and rare-earth impurity ions in $YAlO_3$

2006 J. Phys.: Condens. Matter 18 4751

(http://iopscience.iop.org/0953-8984/18/19/026)

INSTITUTE OF PHYSICS PUBLISHING JOURNAL OF PHYSICS: CONDENSED MATTER

J. Phys.: Condens. Matter **18** (2006) 4751–4761 doi:10.1088/0953-8984/18/19/026

Electron paramagnetic resonance studies of cobalt and rare-earth impurity ions in $YAlO_3$

I Stefaniuk[1,5], A Matkovskii[1], C Rudowicz[2], A Suchocki[3], Z Wilamowski[3], T Lukasiewicz[4] and Z Galazka[4]

[1] Institute of Physics, University of Rzeszów, Rejtana 16a, 35-310 Rzeszów, Poland
[2] Institute of Physics, Szczecin University of Technology, Aleja Piastów 17, 70-310 Szczecin, Poland
[3] Institute of Physics, Polish Academy of Sciences, Aleja Lotników 32, 02-668 Warszawa, Poland
[4] Institute of Electronic Materials Technology, Wołczynska 133, 01-919 Warszawa, Poland

E-mail: istef@univ.rzeszow.pl

Received 12 February 2006
Published 27 April 2006
Online at stacks.iop.org/JPhysCM/18/4751

Abstract

The results of X-band electron paramagnetic resonance (EPR) measurements of Co^{2+} ions in $YAlO_3$ (YAP) crystals in the temperature range 1.8–40 K are presented. The temperature and angular dependences of EPR spectra have been analysed using a triclinic spin Hamiltonian (SH) consisting of the electronic Zeeman and hyperfine terms. Two distinct positions α and β are identified for Co^{2+} complexes and ascribed to the substitutional Co^{2+} ions at the Al^{3+} and Y^{3+} sites, respectively. The values of the SH parameters are obtained by least squares fitting the α- and β-type Co^{2+} spectra yielding the principal (orthorhombic-like) values of the tensors g and A as well as the orientation of their principal axes. The additionally observed EPR spectra of the unintentional impurities Nd^{3+} and Er^{3+} in YAP crystals are also analysed.

1. Introduction

Co-doped oxide crystals are attractive materials for 'eye safe' laser operation near 1.5 μm and as nonlinear absorbers for passive Q-switching [1, 2]. EPR and optical spectra as well as nonlinear absorption properties of $Y_3Al_5O_{12}$:Co, $SrLaAlO_4$:Co, $Mg_2Al_2O_4$:Co, $LaGaO_3$:Co, and $SrLaGa_3O_7$:Co were investigated in [2–6]. The EPR spectra of various ions in $YAlO_3$ crystals, e.g. the $3d^N$ ions Cr^{3+}, Ti^{3+}, Mn^{4+}, Mn^{5+} and Fe^{3+} [7–11] and the $4f^N$ ions Er^{3+}, Nd^{3+} and Ce^{3+} [12–14], were also previously studied. In this work we investigate the X-band EPR spectra of Co^{2+} ions in perovskite yttrium aluminate $YAlO_3$ (YAP) crystals in the temperature range 1.8–40 K. We aim to obtain a better insight into the spectroscopic properties of paramagnetic Co centres and structural information about their nearest environment in the

[5] Author to whom any correspondence should be addressed.

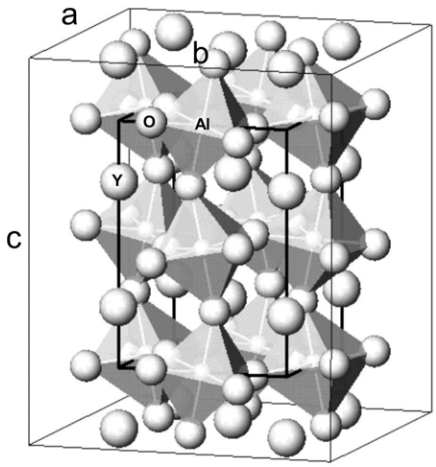

Figure 1. The unit cell of $YAlO_3$ (YAP) crystal.

YAP host. To do this we carried out a detailed analysis of the temperature and angular dependences of EPR spectra using an arbitrarily symmetry spin Hamiltonian (SH), i.e. of the triclinic form. This enabled us to process the experimental data expressed in the crystallographic axis system. Our analysis resulted in the identification of two distinct positions α and β for Co^{2+} complexes, which are ascribed to the substitutional Co^{2+} ions at the Al^{3+} and Y^{3+} sites, respectively. The values of the SH parameters were obtained by least squares fitting the α- and β-type Co^{2+} spectra using the computer program EPR–NMR version 6.5 [15]. These computations yield the principal (orthorhombic-like) values of the tensors g and A as well as the orientation of their principal axes. Additionally, we observed EPR spectra of unintentional impurities Nd^{3+} and Er^{3+} in YAP crystals, which were also analysed and the resulting SH parameters compared with the available literature values [12–14].

2. Crystal structure

The structural data indicate that YAP crystallizes in an orthorhombically distorted perovskite structure with the lattice parameters $a = 0.518$ nm, $b = 0.533$ nm, $c = 0.737$ nm [16–18]. The space group D_{2h}^{16} was chosen to describe the symmetry of the unit cell in YAP crystals using the *Pbnm* group coordinate system [16, 17]. The structure of $YAlO_3$ can be represented (see figure 1) as a grid of tilted AlO_6 octahedra with the Y ions occupying the empty space between the octahedra. The ionic radii of the cations, R, are $R(Y^{3+}) = 0.097$ nm, $R(Al^{3+}) = 0.057$ nm, $R(Co^{3+}) = 0.064$ nm, $R(Co^{2+}) = 0.078$ nm, $R(Nd^{3+}) = 0.099$ nm and $R(Er^{3+}) = 0.085$ nm [19]. It is then expected that Co ions substitute Al cations rather than Y cations in the YAP host.

Four structurally equivalent Al^{3+} sites exist in the YAP unit cell with Al cations located at the centres of nearly perfect AlO_6 octahedra [7]. The bond-length distortion, defined as $(1/n) \cdot \sum \{(r_i - r)/r\}^2 \cdot 10^3$ (r being the average bond-length, r_i an individual bond length and n the number of bonds), was determined as 0.02 [18]. The O–Al–O angles in the respective octahedra vary in the range 89.6°–90.6°. Since the deviations of the respective angles from 90° and the bond-length distortion are small the AlO_6 octahedra may be considered to be only slightly distorted. The immediate surrounding of the Y cations consists of eight oxygen anions, whereas the Y–O bond-lengths in the YO_8 dodecahedra differ one from another, e.g. in the range

from 0.2284 to 0.2597 nm for YAP–1% Nd. Hence, the YO_8 dodecahedra are considerably distorted with a bond-length distortion equal to 3.15 [18].

3. Experimental details

YAP single crystals were grown by the Czochralski method using Oxypuller equipment (Cyberstar, France). The yttrium alumina compound YAP melts congruently at 1870 °C and the growth process is carried out from a stoichiometric composition. Y_2O_3, Al_2O_3 and dopant ions (Co, rare-earth elements) in the form of oxides of purity 4 N (99.99%) were used as raw materials. Thermal system consisted of an yttrium crucible, 50 mm in diameter and height, embedded in zirconia grog and a passive iridium after-heater. Both the crucible and after-heater were insulated with alumina around them. The growth rate was 1–1.2 mm h^{-1} and the rotation rate 10–12 rpm, and a nitrogen atmosphere was used. Stable growth was secured by an automatic diameter control system; the changes in the crystal weight were used as the feedback signal. Single cylindrical crystals, free from inclusions and twin structures, were obtained with diameters up to 25 mm and lengths up to 65 mm.

EPR measurements were performed on the $YAlO_3$:Co samples cut out from the as-grown single crystals in the directions parallel to the crystallographic axes (a, b and c) with the dimensions of $1.5 \times 1 \times 1$ mm^3, respectively. The EPR spectra were investigated in a wide range of temperatures from 40 to 1.8 K using an EPR X-band spectrometer (Bruker ESP-300 with 100 kHz magnetic field modulation). At temperatures higher than 40 K the intensity of the observed EPR spectra gradually decreases and disappears at around 50 K. Measurements at low temperatures were carried out using a helium cryostat (Oxford Instruments ESR-900). The samples were rotated in the resonance cavity using a 1-degree goniometer. Changes of the rotation plane were realized by changing the position of the sample on the sample holder. The accuracy of the sample setting in each new plane was verified by a series of preliminary control measurements, which enabled the EPR spectrum to be compared and matched along one common axis in the new plane with that in the previous plane. Subsequent corrections of the sample setting were made by adjusting the gluing of the sample to the holder.

4. Analysis of EPR spectra

The only naturally abundant Co isotope is ^{59}Co with the nuclear spin $I = 7/2$. The electronic ground state of free $Co^{2+}(3d^7)$ ion is ^4F, which splits in an octahedral crystal field into two orbital triplets $^4T_1$ and $^4T_2$, and a higher singlet $^4A_2$ (see, e.g., [20–23]). Further splitting of the ground triplet $^4T_1$ due to the spin–orbit coupling results in the lowest Kramers doublet with an electronic effective spin $S = 1/2$. This yields EPR spectra of $^{59}Co^{2+}$ ($S = 1/2$) ions with a large anisotropic g-tensor and consisting of eight hyperfine structure components due to $I = 7/2$ [20]. EPR spectra of Co^{2+} ions in YAP are only observed at temperatures below 30 K. A sample EPR spectrum is presented in figure 2 together with a simulation of the EPR spectra for Co^{2+} ions. Measurements of the angular dependences of the EPR spectra were performed in three planes perpendicular to the crystallographic axes a, b and c. Measurements in the b–c and a–c plane were performed at 12 K, and those in the a–b plane below 6 K. A sample angular dependence of the spectra presented in figure 3 shows four groups of EPR lines each consisting of eight lines with comparable large intensity as well as two groups each consisting of eight lines with rather low intensity. Moreover, we also observe (see figure 3) four additional groups of EPR lines of a different character, with two groups positioned in the low magnetic field and the other two groups positioned in slightly higher fields. Each group consists of one strong line and eight associated lines with small intensity.

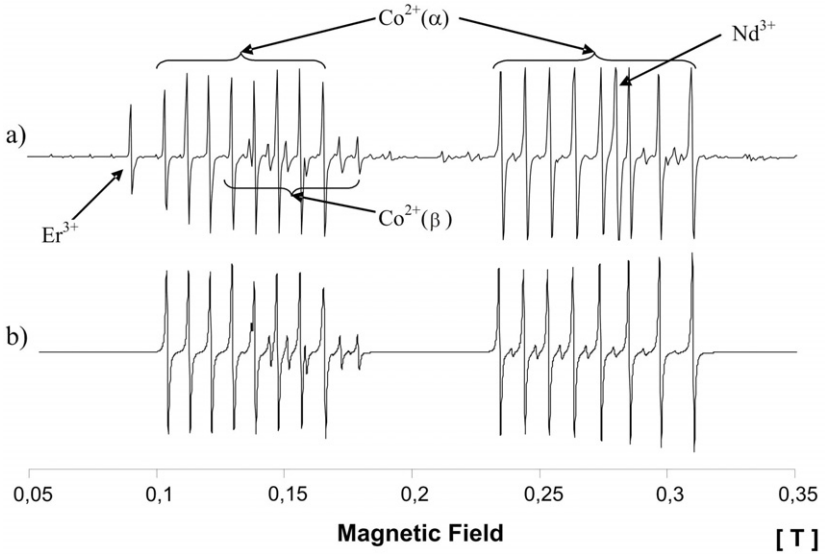

Figure 2. EPR spectra of Co^{2+} ions in YAP crystals at 12 K (*a*–*c* plane, $\varphi = 44°$): (a) experimental spectra and (b) theoretical simulations using the fitted SH parameters in table 1.

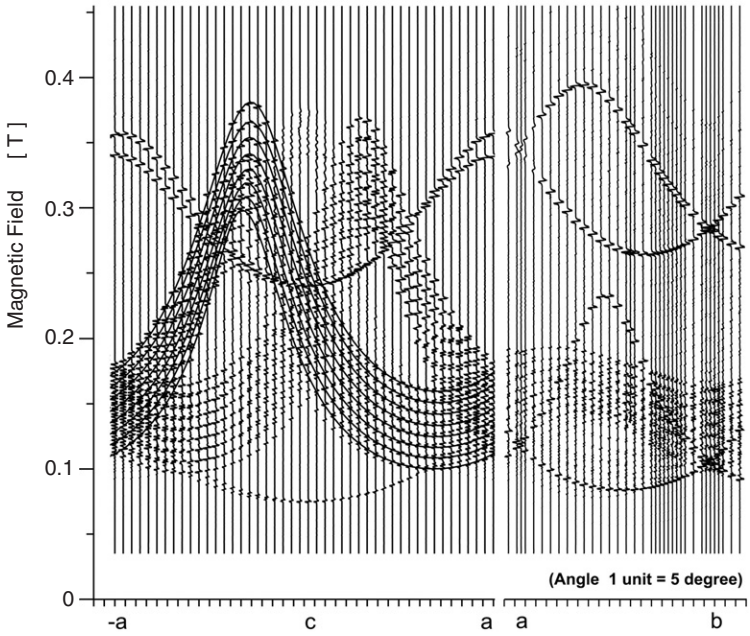

Figure 3. Angular dependence of the EPR spectra with the magnetic field in the *b*–*a* plane (at 6 K) and the *c*–*a* plane (at 12 K); theoretical simulations using the fitted SH parameters in table 1 are represented by continuous lines.

Analysis of the experimental angular dependences reveals the existence of two different types of Co^{2+} complexes, labelled α and β, both with an effective spin $S = 1/2$. The α-complex spectra exhibit visible strong hyperfine structure. Four sets of lines due to the

transitions between the lowest Kramers doublet levels with $M_s = \pm 1/2$ were observed. Since the crystallographic structure of YAP shows four equivalent positions occupied by Al ions in the four Al–O pseudo-cells, the α-type spectra can be attributed to Co^{2+} ions located at the octahedrally coordinated Al sites. Moreover, the orientation of the pseudo-cells with respect to the crystallographic axes corresponds to the observed angular dependences of the Co^{2+} EPR spectra for the α complex. Similar spectra of Co ions at octahedral sites were also observed in $SrLaGa_3O_7$ (SLGO), $SrLaAlO_4$ (SLA) and $CaTiO_3$ crystals [5, 6, 24]. The spectra of the β complex exhibit a visible hyperfine structure of weak intensity and only two sets of EPR lines are observed. The analysis of the angular dependences of the β-type spectra and the crystallographic data suggests that the Co(β) ions occupy two crystallographically equivalent positions in the unit cell. Hence, the β complex can be tentatively attributed to Co^{2+} ions located at the Y^{3+} sites with C_s local site symmetry.

The EPR spectra of both $Co^{2+}(\alpha)$ and $Co^{2+}(\beta)$ complexes as well as the Er^{3+} ions can be described by a general, i.e. triclinic, SH with $S = 1/2$ and $I = 7/2$ [5, 20, 21, 23]:

$$H = \mu_B B \cdot g \cdot S + S \cdot A \cdot I, \tag{1}$$

where μ_B is the Bohr magneton and g and A are the Zeeman and hyperfine structure tensors. The SH parameters g_{ij} and A_{ij} were determined using the computer program EPR–NMR (version 6.5 [15]). Analysis of the EPR spectra and the fittings were performed assuming the local site symmetry C_i for the $Co^{2+}(\alpha)$ complex, whereas C_s was assumed for the $Co^{2+}(\beta)$ complex and Er^{3+} ions. The triclinic symmetry implies the non-coincidence of the principal axes of the tensors g and A in the former case, whereas for the monoclinic symmetry one principal axis of the tensors g and A should be coincident in the latter case. While the non-coincidence in question is observed for the $Co^{2+}(\alpha)$ complex, only a near coincidence of the principal y-axis is noted for the $Co^{2+}(\beta)$ complex (see below). This may either indicate some additional distortions and lowering of the monoclinic symmetry at the $Co^{2+}(\beta)$ sites or arise from the computational procedure within the EPR–NMR program.

The angular dependences in the three mutually perpendicular planes were taken into account, yielding over 300 experimental data points used for fittings for each complex. As an additional check-up, a comparison was made of the experimental angular dependences taken in a fourth plane inclined at a certain angle w.r.t. the three orthogonal planes with the corresponding ones simulated using the fitted SH parameter values. A good agreement obtained in this comparison enabled us, even without detailed fittings, to verify the reliability of the components of the tensor g and A determined from fittings in the basic three planes and thus the final principal directions and the principal g_{ii} and A_{ii} values for the two complexes. In table 1 we list the components g_{ij} and A_{ij} expressed in the laboratory, i.e. crystallographic (a, b, c), axis system as well as the principal (orthorhombic-like) values g_{ii} and A_{ii} and the orientation of the corresponding principal axes for the complex $Co^{2+}(\alpha)$ and $Co^{2+}(\beta)$. Taking into account the accuracy of the EPR–NMR program fittings ($\sim 0.2^\circ$) and the measurement errors, the uncertainty of the polar angles in table 1 is estimated as about 0.5°–1.0°.

EPR spectra due to Nd^{3+} and Er^{3+} ions were also identified in our YAP crystal. The present analysis enables comparison with earlier results for YAP crystal doped with Nd^{3+}, Er^{3+} and Ce^{3+} [12–14] as well as verification of the orientation of our crystal. An analysis of EPR spectra of Nd^{3+} in YAP crystal was presented earlier [25]; however, for comparison we also include these data in table 2. For Nd^{3+} and Er^{3+} ions we provide in table 2 the polar angles θ_z and φ_z, since only these angles are available in the respective references whereas other polar angles are available for the Nd^{3+} data in [25] and the present Er^{3+} data (see below). Note that in [25]the SH parameters were inadvertently named the '*crystal field parameters*', which constitutes another case of widespread confusion—for details see the reviews [26, 27]. Natural

Table 1. The spin Hamiltonian parameters determined from EPR spectra for the $Co^{2+}(\alpha)$ and $Co^{2+}(\beta)$ complexes in $YAlO_3$ crystals. A_{ij} is in units of (10^{-4} cm^{-1}) and polar angles in degrees (with an uncertainty of about 0.5°).

	g_{ij}				A_{ij}				
j	x	y	z	Principal values	j	x	y	z	Principal values
				$Co^{2+}(\alpha)$					
g_{xj}	4.31(1)	−0.42(1)	1.50(1)	5.42(1)	A_{xj}	157(1)	14(1)	36(1)	288(1)
g_{yj}		4.92(1)	1.16(1)	5.02(1)	A_{yj}		140(1)	−81(1)	164(1)
g_{zj}			2.34(1)	1.13(1)	A_{zj}			237(1)	82(1)
θ	118.0	74.9	147.5		θ	29.9	91.4	119.8	
φ	248.2	330.0	34.9		φ	292.9	205.4	296.2	
				$Co^{2+}(\beta)$					
g_{xj}	5.99(1)	1.22(1)	0.24(1)	6.67(1)	A_{xj}	135(1)	47(1)	−2.0(5)	178(1)
g_{yj}		4.35(1)	0.24(1)	3.70(1)	A_{yj}		126(1)	4.1(5)	84(1)
g_{zj}			1.83(1)	1.81(1)	A_{zj}			−8.5(5)	−8.7(5)
θ	86.1	87.2	4.8		θ	89.6	87.3	2.7	
φ	28.1	118.3	244.2		φ	42.3	132.3	304.0	

Table 2. The spin Hamiltonian parameters determined from EPR spectra for the Nd^{3+} and Er^{3+} ions in $YAlO_3$ crystals. The principal values of A_i are in units of (10^{-4} cm^{-1}) and the polar angles are in degrees.

	$^{143}Nd^{3+}$				$^{145}Nd^{3+}$	Er^{3+}			
g_x	2.799(4)	2.83(1)	1.693	2.812(5)	2.812(5)	8.98(1)	2.81	8.954(5)	8.925(4)
g_y	2.539(3)	2.58(1)	2.57	2.554(5)	2.554(5)	8.13(1)	8.162	8.128(5)	8.038(3)
g_z	1.713(2)	1.69(1)	2.82	1.700(2)	1.700(2)	2.73(1)	9.213	2.787(2)	2.896(2)
A_x	273(10)	295	298	212.6(5)	131.7(5)	329	280	70.0(5)	312(10)
A_y	228(10)	256	258	217.9(5)	103.7(5)	315	335	74.2(5)	311(10)
A_z	215(10)	192	192	206.3(5)	147.1(5)	250	350	167.8(5)	230(10)
θ_z	89.0	90	90	90	90	90	90	90	90.2(5)
φ_z	29.8	30.5	30.5	27.76	27.76	41. 4	41.4	41.54	40.6(5)
Ref.	[25]	[12]	[13]	[14]	[14]	[12]	[13]	[14]	This work

erbium, in addition to even isotopes with zero nuclear spin, also contains an odd isotope ^{167}Er with the nuclear spin $I = 7/2$ [12, 20]. The experimental EPR spectrum of the Er^{3+} ion, with the electronic configuration $4f^{11}$ and the ground state $^4I_{15/2}$, agrees very well with the theoretical predictions [20]. The X-band EPR spectra are ascribed to the substitutional Er^{3+} ions at Y^{3+} sites [12].

For the Er^{3+} ions the fittings using the EPR–NMR program were performed only for the g tensor. The results are:

(i) g_{ij} in the crystallographic axis system: $g_{xx} = 5.068$, $g_{xy} = 2.542$, $g_{xz} = 0.037$, $g_{yy} = 5.872$, $g_{yz} = 0.070$, $g_{zz} = 8.918$,
(ii) the principal values g_i: $g_x = 8.925(4)$, $g_y = 8.038(3)$, $g_z = 2.896(2)$, and
(iii) the polar angles in degrees: $\theta_x = 5.0(5)$, $\varphi_x = 128.7(5)$, $\theta_y = 95.0(5)$, $\varphi_y = 130.6(5)$, $\theta_z = 90.2(5)$, $\varphi_z = 40.6(5)$.

Because of the low line intensity of the hyperfine structure and the overlap of these lines with those due to cobalt ions, it was impossible to carry out complete parameter fittings

using the EPR–NMR program for Er^{3+} ions. The large difference between the intensity of hyperfine structure lines and the strong associated single line intensity is due to the small amount (22.95%) of the Er isotope with nuclear spin equal to 7/2 within the total number of Er ions. The components of the hyperfine structure tensor A_{ij} for Er^{3+} ions were obtained by least squares fittings using a separate Maple/Excel program based on equation (1). The coincidence of the principal axes of the tensors g and A was assumed in these computations. The fitted SH parameter values for Er^{3+} ions, together with other pertinent literature data for comparison [12–14, 25], are also listed in table 2.

The quality of the fitted SH parameters for the $Co^{2+}(\alpha)$ and $Co^{2+}(\beta)$ complex in table 1 was also checked by simulations of EPR spectra carried out using the EPR–NMR program [15]. Comparison of the experimental and theoretical EPR spectrum presented in figure 2 indicates that the calculated hyperfine structure lines for Co^{2+} ions agree very well with the experimental results. Figure 3 presents the experimental angular dependences of EPR spectra for the two Co^{2+} complexes together with the dependences simulated using the fitted SH parameters in table 1. For clarity in figure 3 the lines belonging to the $Co^{2+}(\alpha)$ complex are marked only for one orientation.

In order to verify the reliability of the fitted SH parameter values for the $Co^{2+}(\alpha)$ and $Co^{2+}(\beta)$ complex in table 1 we have also reviewed the pertinent listings in [21, 28, 29] and more recent literature data [30–33]. Our components of g_{ij} and A_{ij} for Co^{2+} compare well with pertinent literature data for similar ion–host systems. For example, Co^{2+} ions in octahedrally coordinated sites in, for example, $MSO_4{\cdot}7H_2O$ (M = Ni, Mg; low symmetry sites) [30], $KNbO_3$ (rhombohedral phase, isotropic g and A) and Co^{2+}–V_o (axial $g_\parallel$, $g_\perp$) in $KNbO_3$ and $KTaO_3$ [31], and $LiMPO_4$ (M = Ni, Co, Mg; low symmetry sites) [32]. The principal value of $g_z = 1.13$ for $Co^{2+}(\alpha)$ seems to be rather on the low side as, in general, the smallest components of g_{ii} are around 1.7–1.8 [21, 28–33]. Interestingly, the low symmetry Co centre labelled O_4 in diamond exhibits two principal g values lower than the free electron $g \cong 2$ [33], whereas the values of other parameters g_{ii} and A_{ii} are comparable with the values in table 1. A microscopic spin Hamiltonian theory of g_{ij} (as, for example, of the axial components $g_\parallel$ and $g_\perp$ for Co^{2+} in $KNbO_3$ and $KTaO_3$ [34]) and A_{ij} for the Co^{2+} ion may help to discriminate between reliable and unreliable fitted principal values of the tensors in question. However, to the best of our knowledge, no comprehensive theory exists for low symmetry cases required for Co^{2+} in YAP.

Incidentally, we note that no consistent convention exists in the literature concerning the presentation of the principal g_{ii} and A_{ii} values. Various sequences of the largest to the smallest (1, 2, 3) or (x, y, z) components appear [21, 28–33]. Such a convention could probably be worked out in analogy with the standardization of the zero-field splitting parameters for orthorhombic [35] and lower symmetry [36] (for more recent references, see [27]).

Concerning the fitted SH parameter values for the Nd^{3+} and Er^{3+} ions in table 2, we observe a fair consistency of the g_{ij} and A_{ij} values taken from different authors, apart from some rearrangements of the (x, y, z) components arising from the lack of a consistent convention mentioned above. It is worthwhile noting that the effective g-tensor values for various rare-earth ions in high temperature superconductors have been calculated by Misra *et al* [37] using microscopic spin Hamiltonian theory. However, such calculations relating the g values with appropriate eigenstates and eigenvalues of the rare-earth ions are beyond the scope of this paper. The present study could also be extended to consider the optical properties of the centres under investigations.

The principal directions determined by us for the $Co^{2+}(\alpha)$, $Co^{2+}(\beta)$ and Er^{3+} complexes are presented together with the YAP crystal structure in figure 4. In the case of $Co^{2+}(\alpha)$ ions, all principal directions of the g tensor are oriented towards the six oxygen ligands. We also

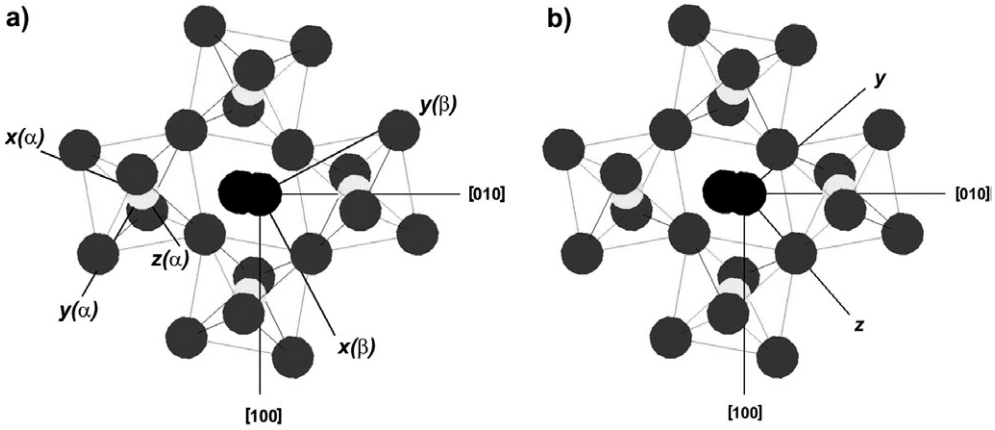

Figure 4. The orientation of the principal axes of the g tensor for: (a) $Co^{2+}(\alpha)$ and $Co^{2+}(\beta)$ complexes and (b) Er^{3+} complex in YAP.

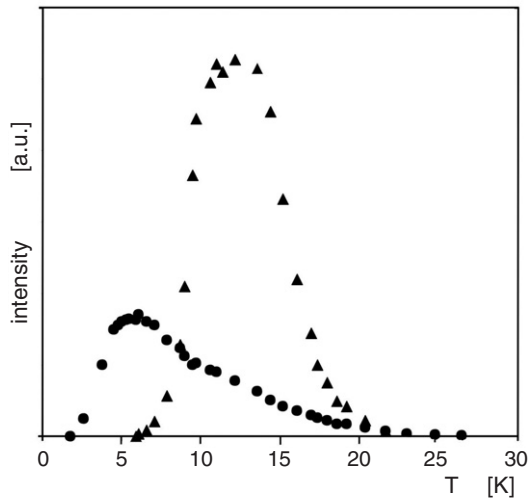

Figure 5. Temperature dependence of the EPR line intensity for the Co^{2+} complexes: α(▲) and β(●), in the a–c plane at $\phi = 64°$ from the a-axis.

note that the principal directions of the g tensor for $Co^{2+}(\beta)$ and Er^{3+} ions are close to each other with one common direction along the [001]-axis being nearly the z-axis for $Co^{2+}(\beta)$, but the x-axis for Er^{3+} ions. This confirms our expectations based on the symmetry arguments. The second principal g direction for the $Co^{2+}(\beta)$ complex and the Er^{3+} one, i.e. the y-axis, is directed towards a nearby oxygen ligand and between two other oxygen ligands. Similarly the third principal g direction is also directed in between two ligands situated above and below this direction.

The intensity of the EPR lines due to Co^{2+} ions has also been measured. The temperature dependences of the EPR spectra (figure 5) reveal distinct characteristics of the two types of Co^{2+} spectra, which are observed in different ranges of temperature. EPR lines due to the α complex appear below 25 K. With temperature gradually lowered, the intensity of these EPR lines increases, reaches a maximum at 12 K, then decreases gradually and disappears at 4 K.

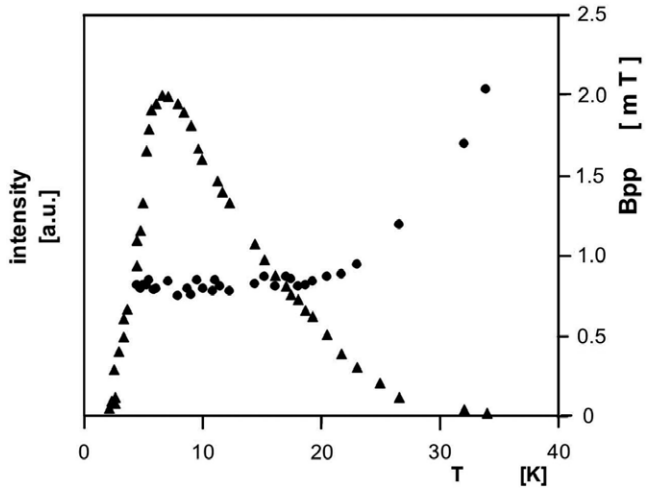

Figure 6. Temperature dependence of the EPR line intensity (▲) and the peak-to-peak line width B_{pp} (●) of Er^{3+} ions in YAP crystal in the a–c plane at $\varphi = 64°$ from the a-axis.

EPR lines due to the β complex appear below 30 K and are observed in a wider temperature range. With temperature gradually lowered, the intensity of these EPR lines increases, reaches a maximum at 6 K, then decreases gradually and disappears at 1.8 K (i.e. the lowest temperature reached by us). The different temperature dependences indicate the different spin–lattice relaxation times, thus confirming the existence of the two distinct Co^{2+} complexes with structurally different environments in the unit cell. It appears that the changes in the EPR line intensity with temperature observed for the $Co^{2+}(\alpha)$ and $Co^{2+}(\beta)$ complexes are close to those for the Nd^{3+} and Er^{3+} ions, respectively.

The temperature dependence of the EPR line intensities and that of the peak-to-peak (B_{pp}) line widths were also measured. From these measurements, the values of the broadening (ΔB) of the EPR lines, i.e. the spin-phonon part of the EPR line width [5], can be determined. The values of ΔB determined from figure 6 for Er^{3+} ions range from 0 at low temperature (1.8 K) to 1.24 (mT) at about 34 K.

The observed line intensity for the Er complex (figure 6) shows behaviour typical of a paramagnetic saturation process. The observed increase in the line widths with increasing temperature can be attributed to the Er^{3+} relaxation time. The estimation of the spin–lattice relaxation time T_1 can be made using the conventional method of line broadening [20] using the expression [5]:

$$T_1^{-1} = 2.8 \times 10^{10} \pi g \Delta B. \tag{2}$$

In the temperature range 1.8–40 K the relaxation time T_1 is governed by the Orbach process [5, 20]:

$$T_1^{-1} = A\left(\exp\left(\frac{\delta}{k_B T}\right) - 1\right)^{-1}, \tag{3}$$

where δ represents the energy splitting between the ground Er^{3+} state and the first excited state, whereas A is a constant characteristic of the Orbach process (in s^{-1}). Figure 7 presents the experimental temperature dependence of T_1 for the Er^{3+} ion in YAP and a theoretical curve fitted using equation (3) with $A = 22 \times 10^{10}$ s^{-1} and $\delta = 154$ cm^{-1}. The EPR line width is

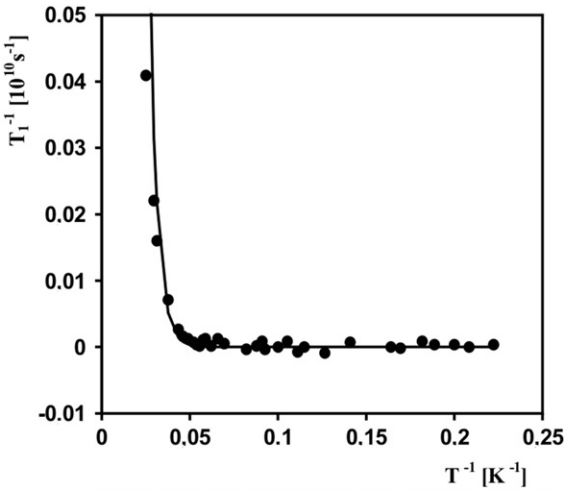

Figure 7. Temperature dependence of the spin–lattice relaxation time T_1 for Er^{3+} ions in YAP crystal; the solid line represents an exponential fit using equation (3) with $A = 22 \times 10^{10}$ s^{-1} and $\delta = 154$ cm^{-1}.

determined by the dephasing time T_2, and therefore the analysis implicitly assumes that in this case the population decay (T_1) dominates the dephasing processes.

5. Conclusions

The results of X-band EPR measurements of $YAlO_3$ (YAP) crystal doped with cobalt ions are presented. The analysis of the various characteristic features of the EPR spectra indicates that the impurity Co^{2+} ions are located at two crystallographically distinct sites, denoted here as the $Co^{2+}(\alpha)$ and $Co^{2+}(\beta)$ complexes. The $Co^{2+}(\alpha)$ and $Co^{2+}(\beta)$ ions are identified as occupying the Al^{3+} and Y^{3+} positions, respectively, in the unit YAP crystal cell. The spin Hamiltonian parameters, including the components of the Zeeman and hyperfine structure tensors g_{ij} and A_{ij}, are experimentally determined by least square fittings of the EPR spectra for both Co^{2+} complexes as well as the Er^{3+} ions. The principal values of the tensors g and A as well as the orientation of their principal axes are also determined w.r.t. the crystallographic axis system. Comparison of the directions of the local magnetic axes with the bond directions in the crystal structure shows a god agreement. The spin Hamiltonian parameters for the impurity Nd^{3+} [25] and Er^{3+} ions determined by us agree well with those reported earlier [12–14]. Fitting the experimental temperature dependence of the spin–lattice relaxation time T_1 for Er ions using an exponential curve yields the coefficients $A = 22 \times 10^{10}$ s^{-1} and $\delta = 154$ cm^{-1}.

Acknowledgment

This work was partially supported by a grant from the Polish Ministry of Education and Science for the years 2006–2009.

References

[1] Kuck S 2001 *Appl. Phys.* B **72** 515
[2] Mierczyk Z 2000 *Nonlinear Absorbers. The investigation of Features, Technology and Selected Applications* (Warsaw: WAT Press) (in Polish)

[3] Gołąb S, Mierczyk Z and Ryba-Romanowski W 2000 *Phys. Status Solidi* a **179** 463
[4] Yumashev K, Denisov I, Posnov N, Prokoshin P and Mikhailov V 2000 *Appl. Phys.* B **70** 179
[5] Aleshevych P, Berkowski M, Ryba-Romanowski W and Szymczak H 2000 *Phys. Status Solidi* b **218** 521
[6] Kaczmarek M, Berkowski M, Fink-Finowicki J, Kwasny M, Palczewska M and Warchoł S 2000 *Prace ITME* **56** 151 (in Polish)
[7] Yamaga M, Takeuchi H, Han T J and Henderson B 1993 *J. Phys.: Condens. Matter* **5** 8097
[8] Belt R F, Latore J R and Uhrin R 1974 *Appl. Phys. Lett.* **25** 218
[9] Rakhimov R R, Wilkerson A L, Loutts G B, Noginov M A, Noginova N, Lindsay W and Ries H R 1998 *Solid State Commun.* **108** 549
[10] Yamaga M, Yosida T, Henderson B, O'Donnell K and Date M 1992 *J. Phys.: Condens. Matter* **4** 7285
[11] Rakhimov R R, Jackson E M, Jones D E and Loutts G B 2004 *J. Appl. Phys.* **95** 5653
[12] Asatryan G R and Rosa J 2002 *Phys. Solid State* **44** 864
[13] Asatryan G R, Rosa J and Mares J A 1997 *Solid State Commun.* **104** 5
[14] Jablonski R and Frukacz Z 1996 *Acta Phys. Pol.* A **90** 339
[15] McGavin D G, Mombourquette M Y and Weil J A 2002 *Computer Program EPR–NMR version 6.5* Department of Chemistry, University of Saskatchewan, Canada
[16] Geller S and Wood E A 1956 *Acta Crystallogr.* **9** 563
[17] Diehl R and Brant G 1975 *Mater. Res. Bull.* **10** 85
[18] Vasylechko L, Matkovskii A, Savytski D, Suchocki A and Wallrafen F 1999 *J. Alloys Compounds* **291** 57
[19] Bojarski Z, Gigla M, Stroz K and Surowiec M 2001 *Crystallography* (Warsaw: PWN) (in Polish)
[20] Abragam A and Bleaney B 1970 *Electron Paramagnetic Resonance of Transition Ions* (Oxford: Clarendon)
[21] Altshuler S and Kozyrev B M 1974 *Electron Paramagnetic Resonance in Compounds of Transition Elements* (New York: Wiley)
[22] Mabbs F E and Collison D 1992 *Electron Paramagnetic Resonance of d Transition-Metal Compounds* (Amsterdam: Elsevier)
[23] Pilbrow J R 1990 *Transition-Ion Electron Paramagnetic Resonance* (Oxford: Clarendon)
[24] Boldu O J L, Boatner L A and Abraham M M 1989 *J. Chem. Phys.* **91** 5117
[25] Stefaniuk I, Obermayr W, Rozborska M, Matkowski A and Kuzma M 2003 *Mol. Phys. Rep.* **37** 127
[26] Rudowicz C 1987 *Magn. Reson. Rev.* **13** 1
Rudowicz C 1988 *Magn. Reson. Rev.* **13** 335 (erratum)
[27] Rudowicz C and Sung H W F 2001 *Physica* B **300** 1
[28] Buckmaster H A 1983 *Magn. Reson. Rev.* **8** 283
[29] Buckmaster H A 1986 *Magn. Reson. Rev.* **11** 81
[30] Misra S K, Wang C, Han S and Korczak S Z 1987 *Phys. Rev.* B **36** 3542
[31] Possenriede E, Schirmer O F, Donnerberg H J and Hellermann B 1989 *J. Phys.: Condens. Matter* **1** 7267
[32] Goñi A, Lezama L, Barberis G E, Pizarro J L, Arriortua M I and Rojo T 1996 *J. Magn. Magn. Mater.* **164** 251
[33] Twitchen D J, Baker J M, Newton M E and Johnston K 2000 *Phys. Rev.* B **61** 9
[34] Zheng W C and Wu S Y 2002 *Z. Naturf.* a **57** 925
[35] Rudowicz C and Bramley R 1985 *J. Chem. Phys.* **83** 5192
[36] Rudowicz C 1986 *J. Chem. Phys.* **84** 5045
[37] Misra S K, Chang Y M and Felsteiner J 1997 *J. Phys. Chem. Solids* **58** 1